

Surface density of states on semi-infinite topological photonic and acoustic crystals

Yi-Xin Sha ¹, Bo-Yuan Liu,² Hao-Zhe Gao,^{2,3} Heng-Bin Cheng ^{2,3}, Hai-Li Zhang,⁴ Ming-Yao Xia,^{1,*}
Steven G. Johnson ^{5,6} and Ling Lu ^{2,7,†}

¹*Department of Electronics, Peking University, Beijing 100871, China*

²*Institute of Physics, Chinese Academy of Sciences/Beijing National Laboratory for Condensed Matter Physics, Beijing 100190, China*


³*School of Physical Sciences, University of Chinese Academy of Sciences, Beijing 100049, China*

⁴*School of Electronic Science and Engineering, University of Electronic Science and Technology of China, Chengdu 611731, China*

⁵*Department of Mathematics, Massachusetts Institute of Technology, Cambridge, Massachusetts 02139, USA*

⁶*Department of Physics, Massachusetts Institute of Technology, Cambridge, Massachusetts 02139, USA*

⁷*Songshan Lake Materials Laboratory, Dongguan, Guangdong 523808, China*

 (Received 5 June 2021; revised 20 August 2021; accepted 24 August 2021; published 17 September 2021)

The iterative Green's function, based on a cyclic reduction of block-tridiagonal matrices, has been the ideal algorithm, through tight-binding models, to compute the surface density of states of semi-infinite topological electronic materials. In this paper, we apply this method to photonic and acoustic crystals, using finite-element discretizations and a generalized eigenvalue formulation, to calculate the local density of states on a single surface of semi-infinite lattices. Three-dimensional examples of gapless helicoidal surface states in Weyl and Dirac crystals are shown and the computational cost, convergence, and accuracy are analyzed.

DOI: [10.1103/PhysRevB.104.115131](https://doi.org/10.1103/PhysRevB.104.115131)

I. INTRODUCTION

Topological classical waves are an exciting focus of recent research [1–4] whose key features are gapless and robust topological surface states at the interfaces. However, there has been no well-established numerical methods to compute a single topological interface state between semi-infinite three-dimensional (3D) bulk crystals made of continuous material. In this paper, we adopt the block-tridiagonal iterative Green's function method to achieve this goal.

The current dominant approach for calculating these states has been to compute the frequency eigenvalues (band structures) of finite-thickness supercells (“slabs”). Although easy to understand and implement, this slab method has several limitations. First, there are *two* surfaces on each slab. One has to disentangle the two surface states by checking their wave functions. Second, large supercells may be required to minimize the coupling between surface states localized on opposite surfaces, greatly increasing the computational costs. Third, it is not convenient to obtain isofrequency cuts of the band diagram, which is required to verify the topological properties such as surface arcs and to compare with the related field-scan experiments [5,6].

It would be ideal to compute the states of a single surface on semi-infinite bulk cells. The effective approach is to compute the local density of states (LDOS) on the surface through the Green's functions [7–10]. Many techniques [11] have been developed for the Green's functions in semi-infinite systems including the recursive method [12,13], transfer-matrix method [14–16], and iterative method [17,18]. All these methods divide the semi-infinite bulk into layers below the surface.

The recursive method writes the Green's function in the form of a continued fraction by relating the neighboring layers. Only a relatively small matrix, describing each layer, is inverted in each recursion and the effective system size grows layer by layer. For example, a recursive scheme based on a finite-difference discretization was used to compute the edge mode of a semi-infinite two-dimensional (2D) photonic crystal [19]. The recursive method is quite general in that each bulk layer can be distinct, i.e., the medium need not be periodic in the direction orthogonal to the surface.

If the semi-infinite bulk cells are all identical, which is the case for periodic lattices, more efficient methods have been developed such as the transfer-matrix and iterative Green's function methods. The transfer-matrix method [14–16] relates the Green's functions of every two neighboring layers with a transfer matrix. By diagonalizing the matrix and obtaining the eigensolutions, the surface Green's function, surface band structure, and surface wave functions can all be constructed. For example, the plane-wave transfer-matrix method was used to study the transmission and edge modes in 2D semi-infinite photonic crystals [20,21]. Unfortunately, the transfer matrix is non-Hermitian and the eigenvector basis can be ill conditioned near an exceptional point [22]. Furthermore, solving eigenvectors is much slower than matrix inversions and the size of the transfer matrix is twice as large as that of a single repeating bulk layer.

The iterative Green's function method [17,18] is the most efficient and is the one used in this paper. The basic idea illustrated in Fig. 1 is to relate the Green's functions of every even layers, by removing the odd ones, so that the surface layer couples with the 2^i layers after i iterations. As a result, the surface Green's function quickly decouples spatially from the bulk and can be solved independently. Historically, a similar iterative technique was proposed for rapidly solving linear systems composed of block-cyclic tridiagonal

*myxia@pku.edu.cn

†linglu@iphy.ac.cn

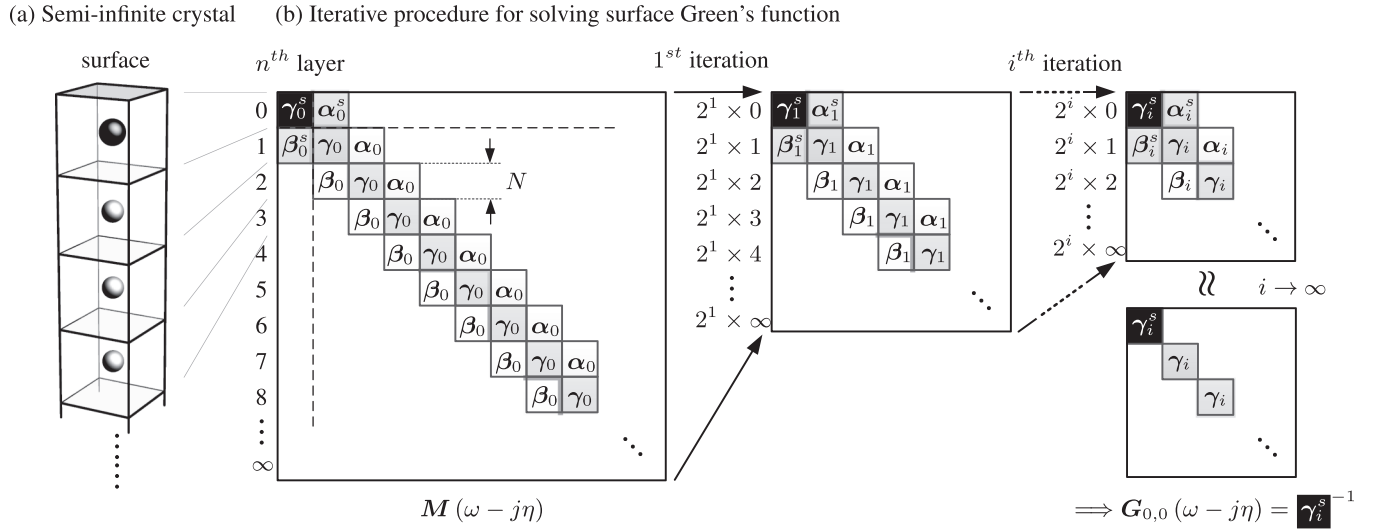


FIG. 1. The iterative Green's function method. (a) Schematic of a semi-infinite crystal. Each cell represents a crystal layer and the top gray surface is the surface boundary. The surface cell can be different from the rest. (b) Iterative procedure for solving the surface Green's function. The block elements (α , β , and γ) are relabeled from $M_{i,j}$ in Eqs. (4) and (5b). After each iteration, half the number of blocks is eliminated and the matrix size is halved. When the off-diagonal blocks are sufficiently small, after enough iterations, the Green's function can be obtained by inverting the remaining diagonal blocks.

(block-Toeplitz) matrices [23–26]. Recently, it has been a standard method for evaluating topological surface states in electronic systems through simplified tight-binding models in a standard eigenvalue problem [27–30].

We note that the semi-infinite periodic media can also be simulated by implementing the outgoing (radiation) boundary conditions in the bulk medium. Unfortunately, the most popular numerical techniques for absorbing boundaries, the perfectly matched layers (PMLs), fail in periodic media [31]. The difficulty lies in the fact that the analytical wave solutions in the periodic medium are not known in general. In this regard, methods such as nonlinear coordinate transforms [32], adiabatic absorbers [31], and the Dirichlet-to-Neumann approach [33] have been developed and numerical examples are all given in 2D.

In this paper, we implement the iterative Green's function method for photonic and acoustic crystals through regular finite-element meshing in a generalized eigenvalue problem. Topological surface states of 3D Weyl and Dirac crystals are calculated for demonstration and the computational performances are discussed in the end.

II. LDOS AND GREEN'S FUNCTION

The source-free Maxwell's equations can be written as a frequency-domain eigenproblem for electric field \mathbf{E} . The sound wave equation in fluids can also be expressed in the same form for acoustic pressure p . Both governing equations for electromagnetics and acoustics can be unified into a generalized eigenvalue problem with ω^2 as the eigenvalue in Eq. (1),

$$\left. \begin{aligned} \nabla \times (\boldsymbol{\mu}^{-1} \cdot \nabla \times \mathbf{E}) &= \omega^2 \boldsymbol{\varepsilon} \cdot \mathbf{E} \\ \nabla \cdot (\rho^{-1} \nabla p) &= -\omega^2 K^{-1} p \end{aligned} \right\} \mathbf{A}\mathbf{u} = \omega^2 \mathbf{B}\mathbf{u}, \quad (1)$$

where $\boldsymbol{\varepsilon}$, $\boldsymbol{\mu}$, ρ , and K are the permittivity, permeability, mass density, and bulk modulus of the material, respectively. \mathbf{A} is the differential operator ($\nabla \times \boldsymbol{\mu}^{-1} \cdot \nabla \times$ or $\nabla \cdot \rho^{-1} \nabla$), \mathbf{B} is the material parameter ($\boldsymbol{\varepsilon}$ or $-K^{-1}$), and \mathbf{u} is the eigenstate (\mathbf{E} or p).

The Green's function, the solution to a differential equation excited by a Dirac delta source, in our system is

$$(\omega^2 \mathbf{B} - \mathbf{A})\mathbf{G}(\omega) = \mathbf{M}(\omega)\mathbf{G}(\omega) = \mathbf{I}, \quad (2)$$

where \mathbf{I} is the identity operator.

LDOS, the key physical quantity to compute in this work, describes the response of a point source (the power emitted by a dipole). It can be written in terms of an imaginary part of \mathbf{G} by imposing an infinitesimal imaginary frequency η [8–10]. η has to be introduced in lossless Hermitian systems, so that the poles in the Green's function [$\mathbf{G}(\omega) = \mathbf{M}(\omega)^{-1}$] broaden to finite values for numerical evaluation. For vector fields, the Green's function is dyadic, and one sums the field components by taking the trace:

$$\text{LDOS}(\mathbf{r}; \omega) = \frac{2\omega}{\pi} \text{Tr} \left\{ \text{Im} \left[\mathbf{B}(\mathbf{r}) \cdot \lim_{\eta \rightarrow 0^+} \mathbf{G}(\mathbf{r}, \mathbf{r}; \omega - j\eta) \right] \right\}. \quad (3)$$

We emphasize that this definition, as well as this work, applies to any frequency-independent material parameters including lossy and gyrotropic terms. \mathbf{B} is usually required to be positive definite for LDOS to be a non-negative real number.

III. ITERATIVE GREEN'S FUNCTION METHOD

By discretizing the system with finite elements [34–36] (edge elements are employed in photonic systems to avoid fake modes), we obtain the semi-infinite

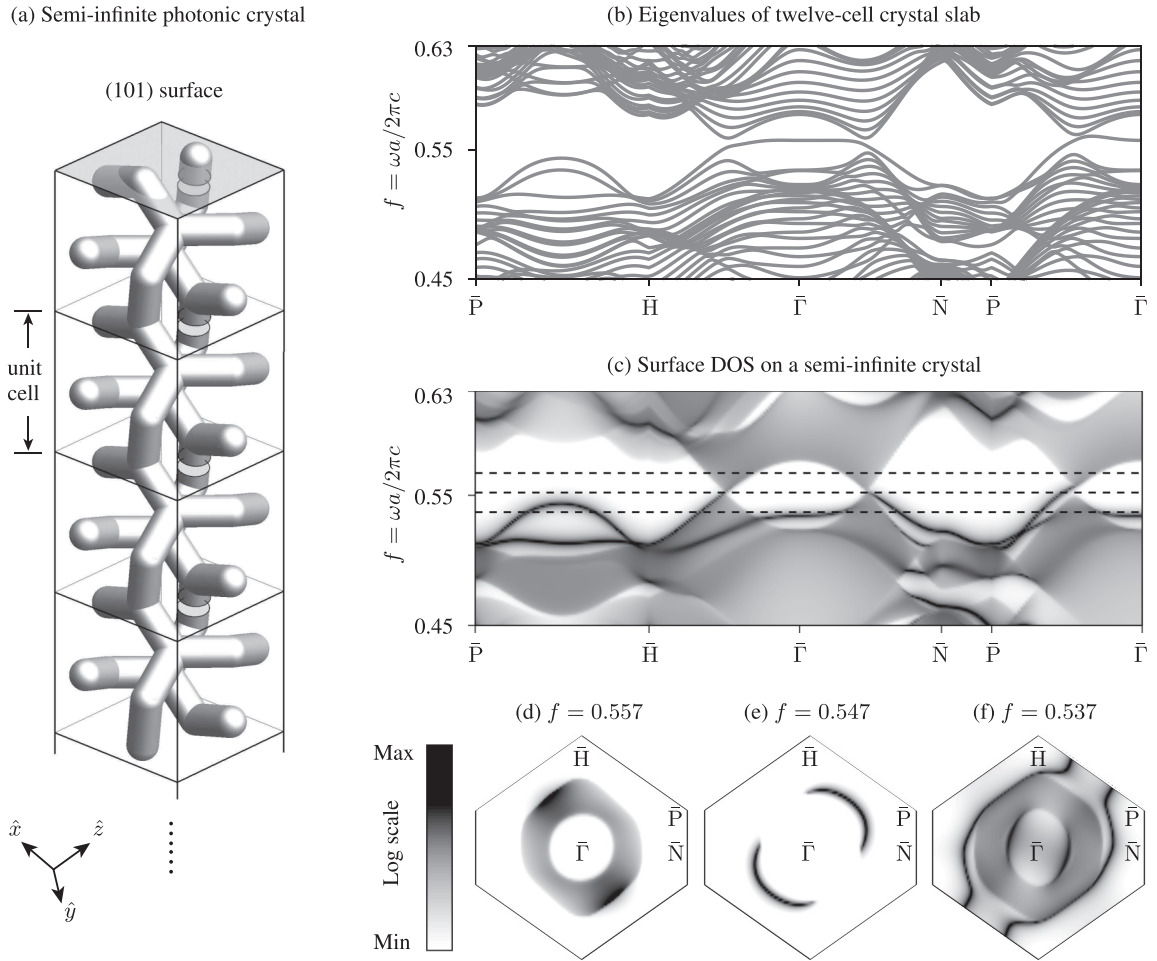


FIG. 2. Surface DOS on a semi-infinite Weyl photonic crystal. (a) Geometry of semi-infinite dielectric photonic crystals with a relative permittivity of 16. The top gray surface is the perfect electric conductor, which satisfies $\hat{n} \times \mathbf{E} = \mathbf{0}$ and \hat{n} is the surface normal. Here, we use cylinders with a radius of $0.10a$ to approximate the double-gyroid structures and an air cylinder with a height of $0.07a$ to break the inversion symmetry, where a is the lattice constant. (b) Band structure of the 12-cell photonic crystal slab with perfect electric conductors on both surfaces. The Weyl points are at the normalized frequency 0.55. (c) Surface DOS on semi-infinite bulk cells. (d)–(f) The isofrequency cuts at normalized frequencies 0.567, 0.552, and 0.537.

eigenmatrix:

$$\mathbf{M}(\omega - j\eta) = (\omega - j\eta)^2 \mathbf{B} - \mathbf{A}$$

$$= \begin{pmatrix} \mathbf{M}_{0,0} & \mathbf{M}_{0,1} & & & & & \\ \mathbf{M}_{1,0} & \mathbf{M}_{1,1} & \mathbf{M}_{1,2} & & & & \\ & \mathbf{M}_{2,1} & \mathbf{M}_{1,1} & \mathbf{M}_{1,2} & & & \\ & & \ddots & \ddots & \ddots & \ddots & \\ & & & \mathbf{M}_{2,1} & \mathbf{M}_{1,1} & \mathbf{M}_{1,2} & \\ & & & & \ddots & \ddots & \ddots \end{pmatrix}. \quad (4)$$

\mathbf{M} is block-cyclic tridiagonal and the subscripts represent the layer numbers. The diagonal block $\mathbf{M}_{n,n}$ represents the intracoupling matrix of the n th layer. The off-diagonal blocks $\mathbf{M}_{n,n+1}$ and $\mathbf{M}_{n+1,n}$ denote the intercoupling matrix between the neighboring layers, whose meshes are joined only at the layer boundaries. These bulk block matrices are identical to $\mathbf{M}_{1,1}$, $\mathbf{M}_{1,2}$, and $\mathbf{M}_{2,1}$, due to the semi-infinite crystal periodicity. In order to fully accommodate the realistic conditions

for the sample surfaces, the surface layer ($n = 0$) is assumed here to be *arbitrarily* different from the inner bulk layers in its thickness, materials, and geometry.

We now derive the surface Green's function $\mathbf{G}_{0,0}$ using Eqs. (2) and (4). Multiplying \mathbf{M} by the zeroth block row of the matrix \mathbf{G} , we get a series of chain equations,

$$\begin{cases} -\gamma_0^s \mathbf{G}_{0,0} = -\mathbf{I} + \alpha_0^s \mathbf{G}_{1,0}, \\ -\gamma_0 \mathbf{G}_{1,0} = \beta_0^s \mathbf{G}_{0,0} + \alpha_0 \mathbf{G}_{2,0}, \\ -\gamma_0 \mathbf{G}_{n,0} = \beta_0 \mathbf{G}_{n-1,0} + \alpha_0 \mathbf{G}_{n+1,0} \quad (n \geq 2), \end{cases} \quad (5a)$$

with

$$\begin{aligned} \alpha_0 &= \mathbf{M}_{1,2}, & \alpha_0^s &= \mathbf{M}_{0,1}, \\ \beta_0 &= \mathbf{M}_{2,1}, & \beta_0^s &= \mathbf{M}_{1,0}, \\ \gamma_0 &= \mathbf{M}_{1,1}, & \gamma_0^s &= \mathbf{M}_{0,0}, \end{aligned} \quad (5b)$$

where α_0 , α_0^s , β_0 , β_0^s , γ_0 , and γ_0^s are the changes in notations for ease of later iterations and the superscript s denotes the sur-

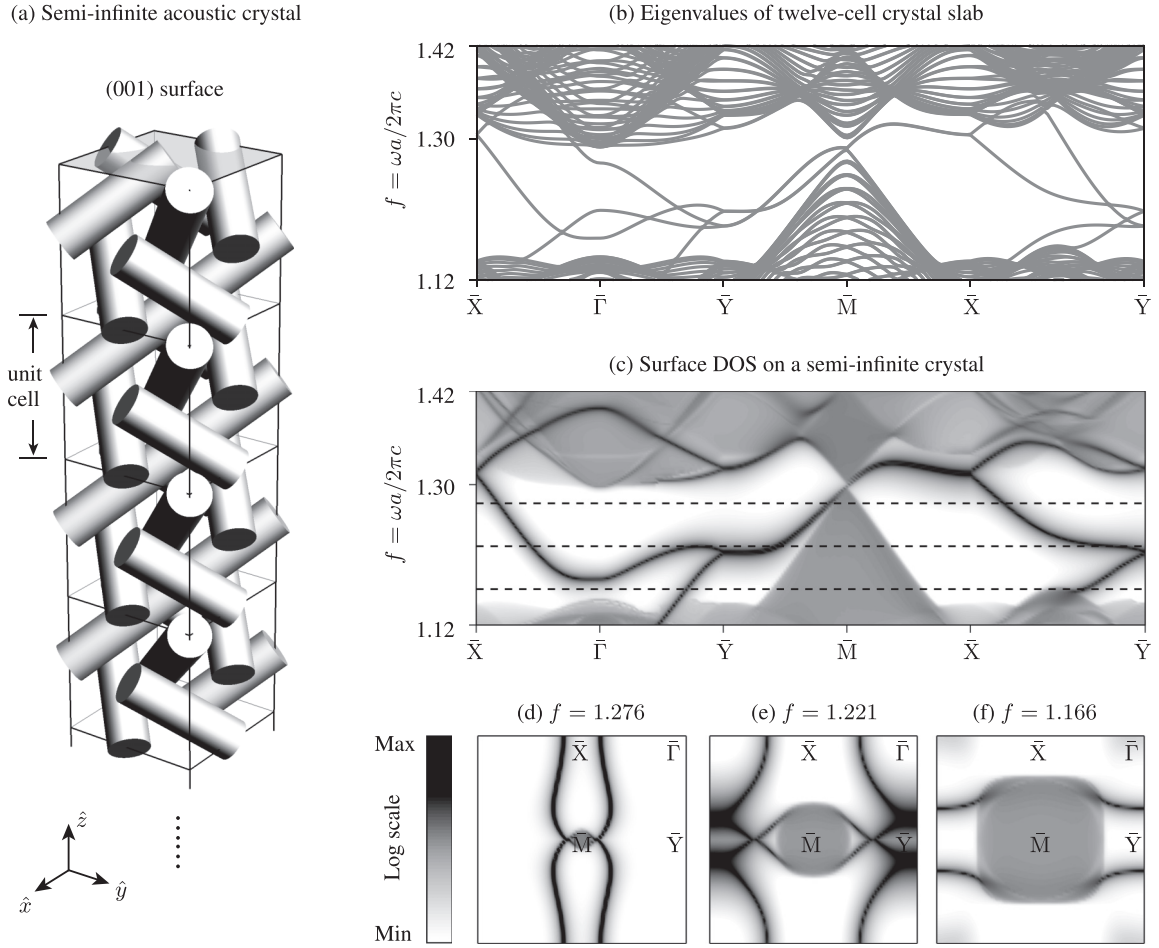


FIG. 3. Surface DOS on a semi-infinite Dirac acoustic crystal. (a) Geometry of the semi-infinite blue-phase-I acoustic crystal. The material is taken as hard wall boundaries in numerics, which satisfies $\hat{\mathbf{n}} \cdot \nabla p = \mathbf{0}$ and $\hat{\mathbf{n}}$ is the surface normal. (b) Band structure of 12-cell acoustic crystal slab with two hard wall boundaries. The Dirac points are at the normalized frequency 1.30. (c) Surface DOS on the semi-infinite bulk cells. (d)–(f) The isofrequency cuts at normalized frequencies 1.276, 1.221, and 1.166.

face layer. By eliminating the odd-layer (odd-index) Green's functions, we update Eq. (5a) as

$$\begin{cases} -\gamma_1^s \mathbf{G}_{0,0} = -\mathbf{I} + \alpha_1^s \mathbf{G}_{2,0}, \\ -\gamma_1 \mathbf{G}_{2,0} = \beta_1^s \mathbf{G}_{0,0} + \alpha_1 \mathbf{G}_{4,0}, \\ -\gamma_1 \mathbf{G}_{2n,0} = \beta_1 \mathbf{G}_{2(n-1),0} + \alpha_1 \mathbf{G}_{2(n+1),0} \quad (n \geq 2), \end{cases} \quad (6a)$$

with

$$\begin{aligned} \alpha_1 &= \alpha_0 (\gamma_0)^{-1} \alpha_0, \\ \alpha_1^s &= \alpha_0^s (\gamma_0)^{-1} \alpha_0, \\ \beta_1 &= \beta_0 (\gamma_0)^{-1} \beta_0, \\ \beta_1^s &= \beta_0 (\gamma_0)^{-1} \beta_0^s, \\ \gamma_1 &= \gamma_0 - \alpha_0 (\gamma_0)^{-1} \beta_0 - \beta_0 (\gamma_0)^{-1} \alpha_0, \\ \gamma_1^s &= \gamma_0^s - \alpha_0^s (\gamma_0)^{-1} \beta_0^s. \end{aligned} \quad (6b)$$

Equation (6a) has half the number of equations in Eq. (5a) but still remains the same structure as Eq. (5a). By repeating this procedure, we obtain the general chain equations,

$$\begin{cases} -\gamma_i^s \mathbf{G}_{0,0} = -\mathbf{I} + \alpha_i^s \mathbf{G}_{2^i,0}, \\ -\gamma_i \mathbf{G}_{2^i,0} = \beta_i^s \mathbf{G}_{0,0} + \alpha_i \mathbf{G}_{2^{i+1},0}, \\ -\gamma_i \mathbf{G}_{2^i n,0} = \beta_i \mathbf{G}_{2^i(n-1),0} + \alpha_i \mathbf{G}_{2^i(n+1),0} \quad (n \geq 2), \end{cases} \quad (7a)$$

with the iterative relations

$$\begin{aligned} \alpha_i &= \alpha_{i-1} (\gamma_{i-1})^{-1} \alpha_{i-1}, \\ \alpha_i^s &= \alpha_{i-1}^s (\gamma_{i-1})^{-1} \alpha_{i-1}, \\ \beta_i &= \beta_{i-1} (\gamma_{i-1})^{-1} \beta_{i-1}, \\ \beta_i^s &= \beta_{i-1} (\gamma_{i-1})^{-1} \beta_{i-1}^s, \\ \gamma_i &= \gamma_{i-1} - \alpha_{i-1} (\gamma_{i-1})^{-1} \beta_{i-1} \\ &\quad - \beta_{i-1} (\gamma_{i-1})^{-1} \alpha_{i-1}, \\ \gamma_i^s &= \gamma_{i-1}^s - \alpha_{i-1}^s (\gamma_{i-1})^{-1} \beta_{i-1}^s. \end{aligned} \quad (7b)$$

The subscript i ($i \geq 1$) means the i th iterations, after which the surface Green's function $\mathbf{G}_{0,0}$ couples with the Green's function $\mathbf{G}_{2^i,0}$ of the 2^i layer. The coupling (off-diagonal)

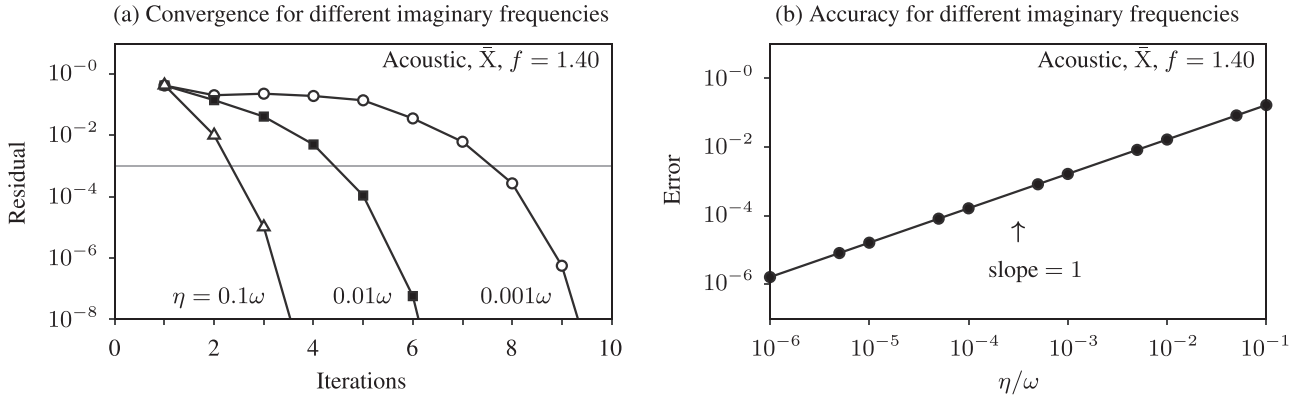


FIG. 4. Numerical convergence and accuracy of the acoustic example. (a) Convergence variance with different imaginary frequencies. The residual is defined as $\|\mathbf{y}_i^s(\eta) - \mathbf{y}_{i-1}^s(\eta)\|_F / \|\mathbf{y}_{i-1}^s(\eta)\|_F$, where i is the iteration step and $\|\cdot\|_F$ represents the Frobenius norm of a matrix. (b) Accuracy dependence on different imaginary frequencies. The error is defined as $\lim_{i \rightarrow \infty} \|\mathbf{y}_i^s(\eta) - \mathbf{y}_i^s(0^+)\|_F / \|\mathbf{y}_i^s(0^+)\|_F$.

matrices α_i^s , α_i , β_i^s , β_i approach zero exponentially fast with the iteration number, so that, after a few iterations, the surface Green's function in Eq. (7a) equals the inverse of the zeroth diagonal block:

$$\mathbf{G}_{0,0}(\omega - j\eta) = \lim_{i \rightarrow \infty} (\mathbf{y}_i^s)^{-1}. \quad (8)$$

The surface-layer DOS is proportional to the trace of $\mathbf{G}_{0,0}$. If the surface layer is identical to the bulk ones, which is the case when the iterative Green's function method was first introduced [17,18], the problem is simplified with $\alpha_i = \alpha_i^s$ and $\beta_i = \beta_i^s$ in Eq. (7b).

Importantly, this iterative approach, solving surface DOS on *one* semi-infinite crystal, can be extended to solve the surface DOS at the interface between *two* semi-infinite crystals. Either of them can also be a semi-infinite homogeneous medium such as air.

IV. NUMERICAL EXAMPLES

Using the above iterative Green's function method, we calculate the surface DOS in semi-infinite 3D topological photonic and acoustic crystals with Bloch-periodic boundary conditions, specified by the Bloch wave vector \mathbf{k} , in the surface-parallel directions. In the surface-normal direction, the crystals are terminated with a perfect electrical conductor or hard wall boundary.

The photonic example, in Fig. 2, is the double-gyroid dielectric photonic crystal [37,38] having four bulk Weyl points and a single helicoid surface state [39]. The surface arcs connecting the four projected Weyl points are plotted in Fig. 2(e).

The acoustic example, in Fig. 3, is the blue-phase-I acoustic crystal having two Dirac points and four helicoid surface states protected by the glide symmetries [6]. The two Dirac points project onto the same point in the surface Brillouin zone attached with four surface arcs, as shown in Fig. 3(d).

The data quality from the semi-infinite crystals is superior, in many ways, to the band structures from the 12-cell slab calculations in Figs. 2(b) and 3(b). First, the surface states from the second surface do not exist in the semi-infinite data. Second, as the bulk level spacing vanishes in the semi-infinite data, one can identify the bulk continuum and the gapless Weyl and Dirac points. Third, the LDOS intensity, measuring

the field localization on the surface, automatically highlights the surface states and compares directly to experiments of near-field scans.

V. COMPUTING EFFICIENCY

The total data points are 125×250 , for the band structures in Figs. 2(c) and 3(c), and 80×80 for the isofrequency cuts in Figs. 2(d)–2(f) and Figs. 3(d)–3(f). The detailed computational costs of each data point (\mathbf{k} , ω) are listed in Table I for one iteration. Different numbers of iterations are required to converge for different data points, typically ranging from three to five iterations when the residual is set to be 10^{-3} and η is set to be 0.01ω in Fig. 4.

Mathematically, introducing the imaginary frequency η is equivalent to doing a frequency average of LDOS in a Lorentzian window [40], where η determines the broadening and the height of the peaks at the poles. If we interpret η as the quality factor $Q = \omega/2\eta$ of the system, $\eta = 0.01\omega$ means $Q = 50$. We linearly scale the η with ω to ensure the same linewidth broadening across the whole spectrum. As shown in Fig. 4, the Green's function converges faster with a larger η , but the error also increases linearly with η .

The computational cost for each iteration grows with N , the number of unknowns in the unit cell as shown in Fig. 1(b). Although the finite-element eigenmatrix \mathbf{M} is sparse, its inverse is not $[\mathbf{y}^{-1}$ in Eqs. 6(b), 7(b), and (8)]. So faster algorithms designed for sparse matrices cannot help and the memory and time costs grow with N^2 and N^3 , as a regular matrix problem. Using 20 Intel Xeon 2.30-GHz processing cores, it takes 10–20 days to obtain the results in Figs. 3(c) and 2(c), and 0.5–1 day to obtain the results in Figs. 3(d)–3(f) and Figs. 2(d)–2(f),

TABLE I. Time and memory costs of the surface DOS calculation for a single data point (\mathbf{k} , ω).

	Photonic	Acoustic
Unit-cell unknowns N	4802	3780
Peak memory (GB)	5.2	3.4
Time per iteration ^a (s)	179.1	90.5

^aMATLAB run using one 2.30-GHz Intel Xeon Gold 6140 processor core.

while it takes no more than half a day to obtain the band structures of a supercell slab as shown in Figs. 3(b) and 2(b). Our approach can be trivially paralleled by distributing the independent data points (\mathbf{k} , ω) on different cores.

VI. CONCLUSION

We implement the iterative Green's function method to calculate the surface density of states in semi-infinite photonic and acoustic crystals. The results are highly desirable for studying the topological states in classical systems, despite the drawback of its large computation costs for 3D problems. This method can be further developed to treat frequency-dependent material parameters [41].

ACKNOWLEDGMENTS

This work was supported by the Natural Science Foundation of China (61531001, 12025409, 11721404, 11974415), by the National Key R&D Program of China (2017YFA0303800), by the Chinese Academy of Sciences through the Project for Young Scientists in Basic Research (YSBR-021), the Strategic Priority Research Program (XDB33000000), and the International Partnership Program with the Croucher Foundation (112111KY5B20200024), by the Beijing Natural Science Foundation (Z200008), and by the Simons Foundation collaboration on Extreme Wave Phenomena.

-
- [1] L. Lu, J. D. Joannopoulos, and M. Soljačić, Topological photonics, *Nat. Photonics* **8**, 821 (2014).
- [2] X. Zhang, M. Xiao, Y. Cheng, M.-H. Lu, and J. Christensen, Topological sound, *Commun. Phys.* **1**, 1 (2018).
- [3] T. Ozawa, H. M. Price, A. Amo, N. Goldman, M. Hafezi, L. Lu, M. C. Rechtsman, D. Schuster, J. Simon, O. Zilberberg *et al.*, Topological photonics, *Rev. Mod. Phys.* **91**, 015006 (2019).
- [4] G. Ma, M. Xiao, and C. T. Chan, Topological phases in acoustic and mechanical systems, *Nat. Rev. Phys.* **1**, 281 (2019).
- [5] B. Yang, Q. Guo, B. Tremain, R. Liu, L. E. Barr, Q. Yan, W. Gao, H. Liu, Y. Xiang, J. Chen *et al.*, Ideal Weyl points and helioid surface states in artificial photonic crystal structures, *Science* **359**, 1013 (2018).
- [6] H. Cheng, Y. Sha, R. Liu, C. Fang, and L. Lu, Discovering Topological Surface States of Dirac Points, *Phys. Rev. Lett.* **124**, 104301 (2020).
- [7] E. N. Economou, *Green's Functions in Quantum Physics* (Springer, Berlin, 2006).
- [8] L. Novotny and B. Hecht, *Principles of Nano-Optics* (Cambridge University Press, Cambridge, UK, 2012).
- [9] A. Oskooi and S. G. Johnson, Electromagnetic wave source conditions, [arXiv:1301.5366](https://arxiv.org/abs/1301.5366).
- [10] W. C. Chew, W. E. Sha, and Q. I. Dai, Green's dyadic, spectral function, local density of states, and fluctuation dissipation theorem, *Prog. Electromagn. Res.* **166**, 147 (2019).
- [11] J. Velez and W. Butler, On the equivalence of different techniques for evaluating the Green function for a semi-infinite system using a localized basis, *J. Phys.: Condens. Matter* **16**, R637 (2004).
- [12] R. Haydock, V. Heine, and M. Kelly, Electronic structure based on the local atomic environment for tight-binding bands, *J. Phys. C* **5**, 2845 (1972).
- [13] R. Haydock, The recursive solution of the Schrodinger equation, in *Solid State Physics* (Elsevier, Amsterdam, 1980), Vol. 35, pp. 215–294.
- [14] D. H. Lee and J. D. Joannopoulos, Simple scheme for surface-band calculations. I, *Phys. Rev. B* **23**, 4988 (1981).
- [15] D. H. Lee and J. D. Joannopoulos, Simple scheme for surface-band calculations. II. The Green's function, *Phys. Rev. B* **23**, 4997 (1981).
- [16] D. H. Lee and J. D. Joannopoulos, Renormalization scheme for the transfer-matrix method and the surfaces of wurtzite ZnO, *Phys. Rev. B* **24**, 6899 (1981).
- [17] M. L. Sancho, J. L. Sancho, and J. Rubio, Quick iterative scheme for the calculation of transfer matrices: Application to Mo (100), *J. Phys. F: Met. Phys.* **14**, 1205 (1984).
- [18] M. L. Sancho, J. L. Sancho, J. L. Sancho, and J. Rubio, Highly convergent schemes for the calculation of bulk and surface Green functions, *J. Phys. F: Met. Phys.* **15**, 851 (1985).
- [19] A. I. Rahachou and I. V. Zozoulenko, Light propagation in finite and infinite photonic crystals: The recursive Green's function technique, *Phys. Rev. B* **72**, 155117 (2005).
- [20] Z.-Y. Li and K.-M. Ho, Light propagation in semi-infinite photonic crystals and related waveguide structures, *Phys. Rev. B* **68**, 155101 (2003).
- [21] M. Che and Z.-Y. Li, Analysis of surface modes in photonic crystals by a plane-wave transfer-matrix method, *J. Opt. Soc. Am. A* **25**, 2177 (2008).
- [22] A. Pick, B. Zhen, O. D. Miller, C. W. Hsu, F. Hernandez, A. W. Rodriguez, M. Soljačić, and S. G. Johnson, General theory of spontaneous emission near exceptional points, *Opt. Express* **25**, 12325 (2017).
- [23] B. L. Buzbee, G. H. Golub, and C. W. Nielson, On direct methods for solving Poissons equations, *SIAM J. Numer. Anal.* **7**, 627 (1970).
- [24] D. Heller, Some aspects of the cyclic reduction algorithm for block tridiagonal linear systems, *SIAM J. Numer. Anal.* **13**, 484 (1976).
- [25] F. Zhang, *The Schur Complement and its Applications* (Springer, Berlin, 2006).
- [26] M. G. Reuter and J. C. Hill, An efficient, block-by-block algorithm for inverting a block tridiagonal, nearly block Toeplitz matrix, *Comput. Sci. Discovery* **5**, 014009 (2012).
- [27] D. E. Petersen, Block tridiagonal matrices in electronic structure calculations, Ph.D. thesis, University of Copenhagen, 2008.
- [28] H. Zhang, C.-X. Liu, X.-L. Qi, X. Dai, Z. Fang, and S.-C. Zhang, Topological insulators in Bi₂Se₃, Bi₂Te₃ and Sb₂Te₃ with a single Dirac cone on the surface, *Nat. Phys.* **5**, 438 (2009).
- [29] Q. Wu, S. Zhang, H.-F. Song, M. Troyer, and A. A. Soluyanov, WannierTools: An open-source software package for novel topological materials, *Comput. Phys. Commun.* **224**, 405 (2018).
- [30] C. Yue, Y. Xu, Z. Song, H. Weng, Y.-M. Lu, C. Fang, and X. Dai, Symmetry-enforced chiral hinge states and surface quantum anomalous Hall effect in the magnetic axion insulator Bi_{2-x}Sm_xSe₃, *Nat. Phys.* **15**, 577 (2019).

- [31] A. F. Oskooi, L. Zhang, Y. Avniel, and S. G. Johnson, The failure of perfectly matched layers, and towards their redemption by adiabatic absorbers, *Opt. Express* **16**, 11376 (2008).
- [32] J. P. Hugonin and P. Lalanne, Perfectly matched layers as nonlinear coordinate transforms: A generalized formalization, *J. Opt. Soc. Am. A* **22**, 1844 (2005).
- [33] S. Fliss and P. Joly, Exact boundary conditions for time-harmonic wave propagation in locally perturbed periodic media, *Applied Numerical Mathematics* **59**, 2155 (2009).
- [34] B. Hiett, Photonic crystal modelling using finite element analysis, Ph.D. thesis, University of Southampton, 2002.
- [35] J.-M. Jin, *The Finite Element Method in Electromagnetics* (Wiley, Hoboken, NJ, 2015).
- [36] A. Bondeson, T. Rylander, and P. Ingelström, *Computational Electromagnetics* (Springer, Berlin, 2012).
- [37] L. Lu, L. Fu, J. D. Joannopoulos, and M. Soljačić, Weyl points and line nodes in gyroid photonic crystals, *Nat. Photonics* **7**, 294 (2013).
- [38] L. Lu, Z. Wang, D. Ye, L. Ran, L. Fu, J. D. Joannopoulos, and M. Soljačić, Experimental observation of Weyl points, *Science* **349**, 622 (2015).
- [39] C. Fang, L. Lu, J. Liu, and L. Fu, Topological semimetals with helicoid surface states, *Nat. Phys.* **12**, 936 (2016).
- [40] X. Liang and S. G. Johnson, Formulation for scalable optimization of microcavities via the frequency-averaged local density of states, *Opt. Express* **21**, 30812 (2013).
- [41] A. Spence and C. Poulton, Photonic band structure calculations using nonlinear eigenvalue techniques, *J. Comput. Phys.* **204**, 65 (2005).